Crystal structure based design of signal enhancement schemes for solid-state NMR of insensitive half-integer quadrupolar nuclei

O'Dell, Luke A.; Ratcliffe, Christopher I.

Publisher's version / Version de l'éditeur:
http://dx.doi.org/10.1021/jp111531e
Journal Of Physical Chemistry A, 115, pp. 747-752, 2011-01-01

THE JOURNAL OF PHYSICAL CHEMISTRY A

ARTICLE

pubs.acs.org/JPCA

Crystal Structure Based Design of Signal Enhancement Schemes for Solid-State NMR of Insensitive Half-Integer Quadrupolar Nuclei

Luke A. O'Dell* and Christopher I. Ratcliffe

Steacie Institute for Molecular Sciences, National Research Council, 100 Sussex Drive, Ottawa, K1A 0R6, Ontario, Canada

Supporting Information

ABSTRACT: A combination of density functional and optimal control theory has been used to generate amplitude- and phase-modulated excitation pulses tailored specifically for the ^{33}S nuclei in taurine, based on one of several reported crystal structures. The pulses resulted in significant signal enhancement (stemming from population transfer from the satellite transitions) without the need for any experimental optimization. This allowed an accurate determination of the ^{33}S NMR interaction parameters at natural abundance and at a moderate magnetic field strength (11.7 T). The ^{33}S NMR parameters, along with those measured from ^{14}N using frequency-swept pulses, were then used to assess the accuracy of various proposed crystal structures.

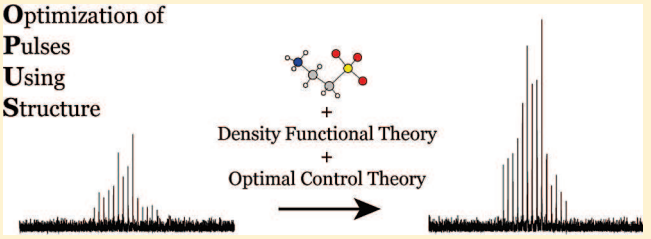

1. INTRODUCTION

There is growing interest in the development of "NMR crystallography",[1] wherein crystal structures can be inferred or refined using a combination of solid-state nuclear magnetic resonance (SSNMR) experiments and ab initio calculations made using density functional theory (DFT). A common approach is to compare experimentally determined parameters (e.g., isotropic chemical shifts, shielding anisotropies, quadrupolar coupling constants)[2−6] with those calculated from crystal structures using gauge-including projector augmented wave (GIPAW) methods,[7−10] which take into account the full periodicity of the crystal lattice. Structures used in these calculations can either have been determined using diffraction methods,[2−6] inferred from the NMR results[11−13] or computationally predicted.[14] SSNMR has several advantages over diffraction techniques, such as the ability to target specific nuclei.[15,16] Its biggest drawback is its low sensitivity, and this is particularly true for the ^{33}S nucleus, which is present in a wide variety of important systems and has the potential to provide valuable information for structure determination or refinement. The ^{33}S isotope has a very low natural abundance (0.76%) and also a low gyromagnetic ratio (γ = 2.06 × 10^7 rad T^{-1} s^{-1}), which translates to a low inherent sensitivity and also limits the maximum radio frequency (RF) power (denoted as a nutation frequency ν_1, in kHz) that can be achieved experimentally. Being a quadrupolar nucleus (spin number I = 3/2), it will also couple to an electric field gradient (EFG), causing anisotropic broadening of the central-transition (CT, +1/2 ↔ −1/2) line shape for all but the most spherically symmetric sulfur environments.[15,16] This complicates spectra as well as further reducing sensitivity.

The low sensitivity of ^{33}S can be overcome in two ways: isotopic enrichment, which can be difficult and expensive, or the use of experimental methods that can enhance the ^{33}S SSNMR signal. Magic-angle spinning (MAS)[15,16] can be used to partially average the second-order quadrupolar interaction (as well as removing other interactions), narrowing the CT powder pattern.[17−19] Spin manipulations, achieved using applied RF control fields (i.e., pulses), can also be used to boost the signal. In particular, irradiation of the satellite transitions (STs, ± 3/2 ↔ ± 1/2) can increase the CT polarization prior to the excitation of the observable single-quantum coherence,[20,21] resulting in a potential enhancement of up to 3 for a spin-3/2 nucleus such as ^{33}S.[22,23] Various reported pulse sequences can accomplish this, including DFS,[24] RAPT,[25] and HS,[26] and these may generally be referred to as "population transfer" (PT) experiments.[20,21] Finally, the "quadrupolar Carr Purcell Meiboom Gill" (QCPMG) protocol, which consists of a repeating loop containing a refocusing pulse and acquisition period, allows a spin−echo to be recorded multiple times per scan.[27,28] Each of these methods (MAS, PT, and QCPMG) can be used in parallel to reduce experiment times by several orders of magnitude[29] and will be essential if natural abundance SSNMR of ^{33}S (or other insensitive quadrupolar nuclei) is to become routine.

MAS and QCPMG experiments are simple to set up, requiring only a calibration of the RF power to set correct pulse lengths. PT schemes, however, require a much more considered approach, with numerous experimental parameters requiring careful optimization. For example, the generation of a DFS pulse shape requires the user to specify the pulse length, power, and initial and final offset frequencies.[24] These frequencies must not approach the CT region too closely or polarization of the CT may be lost. PT experiments can therefore benefit from a prior

Received: December 3, 2010
Revised: December 9, 2010
Published: December 21, 2010

Table 1. ^{33}S NMR Parameters for Taurine Predicted by DFT from an XRD Structure[31] and Measured Experimentally[a]

	C_Q (MHz)	η_Q	δ_{iso} (ppm)	Ω (ppm)	κ	α (°)	β (°)	γ (°)
calcd	1.60	0.85	306	226	−0.54	344	46	3
expt	1.36(2)	0.62(5)	326(1)	186(15)	−0.38(10)	200(5)	64(4)	66(6)

[a] See Supporting Information for parameter definitions.

knowledge of the characteristics of the NMR spectrum, that is, the approximate values of the various NMR interaction parameters such as C_Q and η_Q, which, respectively, describe the magnitude and asymmetry of the quadrupolar interaction. In addition to this, a knowledge of the isotropic chemical shift δ_{iso}, which is the main factor in determining the position of the NMR signal on the frequency axis, eliminates the need to search across the range of possible resonance frequencies to locate the signal, thus, aiding even the simplest single-pulse experiment. DFT calculations, particularly GIPAW approaches,[7−10] can allow reliable predictions of these NMR parameters directly from the crystal structure,[1−13] thereby providing a means of optimizing the SSNMR experiment a priori. In this article, we use one of several reported crystal structures of taurine (2-aminoethanesulfonic acid) to design signal enhancement pulse sequences tailored specifically for the ^{33}S nuclei in this system, with the aim of accurately measuring the ^{33}S NMR interaction parameters at natural abundance and moderate magnetic field strength (11.7 T). This strategy will be referred to as "OPUS" (Optimization of Pulses Using Structure), and we will show that this approach can provide a considerable level of signal enhancement, under both static and MAS conditions, without the need for any experimental optimization. The NMR parameters for the sulfur site in taurine have not previously been reported, so this work constitutes a blind test of this strategy. The resulting experimental parameters are then used to assess the relative accuracies of the various reported crystal structures.

2. EXPERIMENTAL METHODS

The plane-wave DFT calculations were conducted using CASTEP[7−10] in the Materials Studio 4.3 software suite. This software employs the gauge-including projector augmented wave algorithm (GIPAW).[9] Revised Perdew, Burke, and Ernzerhof (PBE) functionals were used with the generalized gradient approximation for the exchange-correlation energy. The plane wave basis set cutoff was set to 550 eV and 8 k-points were sampled. Proton positions were optimized using a Broyden-Fletcher-Goldfarb-Shanno optimization algorithm,[30] with the lattice parameters and coordinates of all other atoms fixed. Ultrasoft pseudopotentials were used for the EFG calculations.[8]

The DFT calculations were first carried out on an XRD structure of taurine (CCSD code TAURIN01),[31] with an optimization of the proton positions prior to the calculation of the NMR parameters. The resulting ^{33}S parameters are presented in Table 1 (see Supporting Information for a list of all reported taurine crystal structures and definitions of the NMR parameters in Table 1). Euler angles were determined using EFGShield.[32] These parameters were used to optimize the ^{33}S NMR experiments.

Rather than attempt to optimize the variables of an existing PT experiment such as DFS, the parameters were instead used to generate unique amplitude- and phase-modulated RF excitation

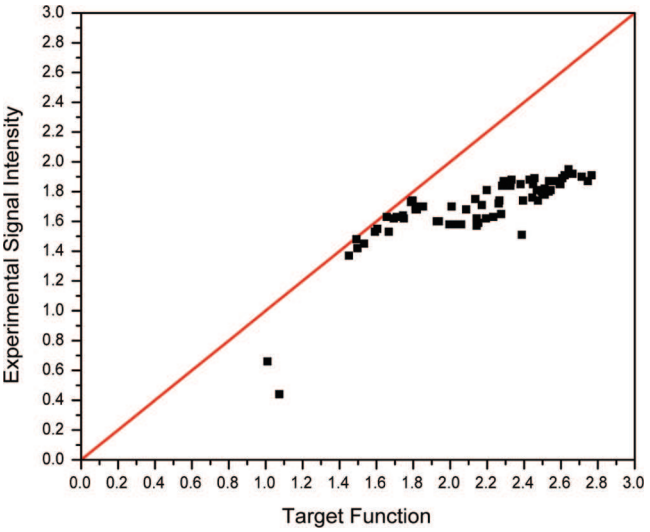

Figure 1. Experimental ^{87}Rb MAS NMR signal intensities obtained from $RbClO_4$ (normalized to that obtained using a standard, CT-selective, $\pi/2$ pulse) vs the target functions of the various OCT-optimized pulses used.

pulses using optimal control theory. The pulse optimizations were carried out with the SIMPSON 2.0 software[33,34] using methods similar to those previously described.[34,35] The spin system was defined using the DFT-predicted ^{33}S NMR parameters in Table 1. The starting operator was set to I1z (thermal equilibrium) and the detection operator was set to I1c, which specifies that only the central transition single-quantum coherence magnitude should be maximized in the optimization. For the iterative optimization procedure itself, pulse lengths were arbitrarily set at either 100 or 200 μs, and element sizes were set to 0.1, 0.2, or 0.25 μs. The RF power was restricted to 30 kHz in all cases due to the relatively long pulse lengths and the low gyromagnetic ratio of ^{33}S. A different, randomly generated pulse was used as the initial shape in each optimization, and each set of pulse parameters was optimized a number of times. Exit tolerances were set to 10^{-4} on the target function and 10^{-3} on the line search, with an initial step size for the bracketing minimum of 10.[34] Powder averaging was achieved using 33 crystal orientations for the MAS experiment and 376 in the static case (orientations calculated using the ZCW algorithm). Five gamma angles were specified for the MAS case. Typically, optimizations converged after about 100 iterations, taking around 1 h on a 2 GHz desktop PC.

To decide which of the numerous optimized pulses to apply experimentally, a test was made of the reliability of the target function (TF) as an indicator of the resulting experimental performance of the pulses. The TF may be considered here as a measure of the simulated performance of the pulse shape.[34] These tests were conducted on a sample of $RbClO_4$ using the ^{87}Rb nucleus under 10 kHz MAS conditions, ^{87}Rb being a far more amenable nucleus to study by SSNMR than ^{33}S. Experimentally determined ^{87}Rb parameters were used for the optimizations.[36] A broad range of pulse lengths and element sizes were optimized using the procedures given above, and the pulses were tested experimentally using an experimental setup as close as possible to that of the ^{33}S experiments (vide infra). The results are plotted in Figure 1. It can be seen that the while the TF is by no means perfectly correlated with experimental performance (likely due to various experimental limitations that are not

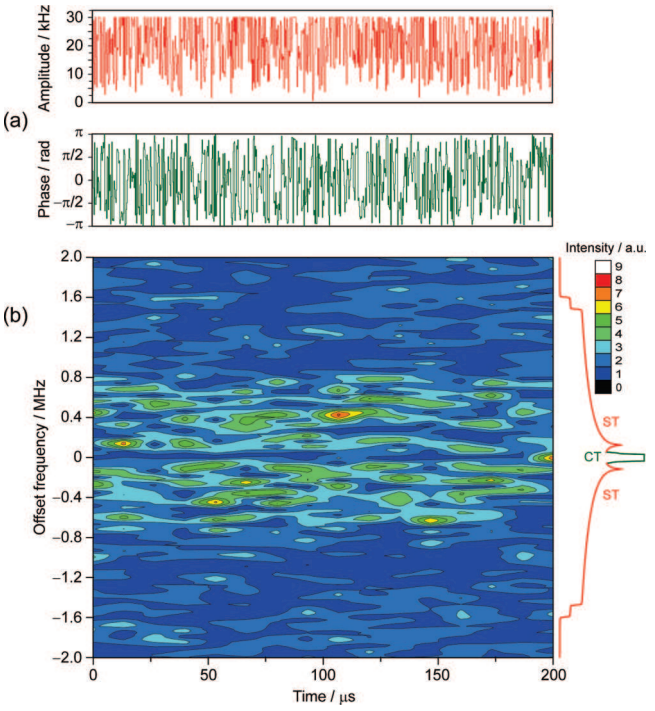

Figure 2. (a) MAS excitation pulse generated using optimal control theory from the DFT-calculated ^{33}S NMR parameters of taurine. (b) Time-resolved Fourier analysis of the pulse. The static ^{33}S ST powder pattern corresponding to the calculated NMR parameters is shown on the right (red) along with the CT (green, truncated).

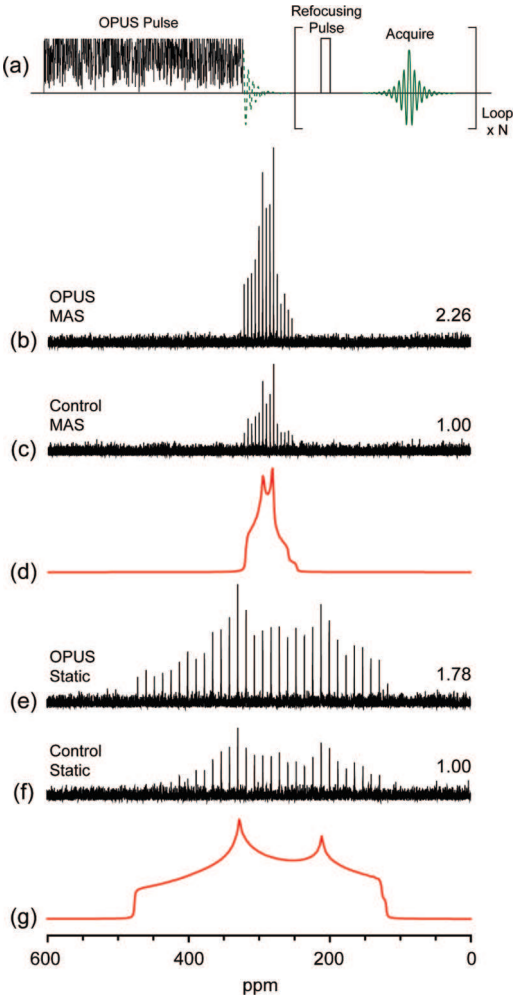

Figure 3. (a) Pulse sequence used. For the control experiments, the OPUS pulse was replaced by a standard pulse. OPUS experiments are shown in (b) and (e) for MAS and static conditions, respectively, and control experiments are shown in (c) and (f). Spectra are in spikelet form due to the use of the QCPMG protocol.[27,28] Relative signal intensities are shown for the MAS and static pairs of spectra. Fitted simulations are shown in (d) and (g) and were made using the Dmfit software.[49].

accounted for in the optimization procedure), the pulses that gave the highest TFs (ca. 2.7) also reliably gave the highest experimental enhancements observed (ca. 1.9). Thus, for the ^{33}S experiments on taurine, the MAS and static pulses with the highest TFs were chosen for the experiments. These target functions were 2.631 and 2.581, respectively, and the full amplitude and phase lists for these pulses are given in the Supporting Information. The amplitudes and phases of the MAS pulse are also plotted in Figure 2a (see section 3 for further discussion).

These OPUS pulses were tested experimentally on a natural abundance sample of ≥99% pure taurine (Sigma Aldrich). A double-resonance, 4 mm Varian probe was used with a Bruker Avance III console and an 11.7 T superconducting magnet ($\nu_L(^{33}S)$ = 38.4 MHz and $\nu_L(^1H)$ = 500 MHz). The RF power on the ^{33}S channel was calibrated using a solution of tetramethylene sulfone in acetone, which was also used as a chemical shift reference (367.55 ppm with respect to CS_2). The transmitter frequency was set to the predicted ^{33}S isotropic chemical shift (306 ppm), which was determined from the calculated isotropic shielding value using an empirical formula reported previously.[37] A QCPMG acquisition loop[27,28] was incorporated after the OPUS pulse, as illustrated in Figure 3a, with standard (rectangular, monochromatic), CT-selective refocusing pulses of 4.17 μs duration and 30 kHz RF power. The first FID (dashed line in Figure 3a) was discarded. The duration of the QCPMG loop was set to 5.0 and 2.2 ms for the 10 kHz MAS and static experiments, respectively. In all cases, 100 echoes were acquired with continuous-wave ^{1}H decoupling of about 20 kHz applied for the duration of each scan (including during the OPUS pulses). For comparison purposes, control experiments were conducted by replacing the OPUS pulses with standard CT-selective excitation pulses of 4.17 μs duration and 30 kHz RF power, and all other conditions were left unaltered. Because there exists no straightforward, quantitative way to predict nuclear spin relaxation rates directly from a crystal structure, a value of 4 s was chosen for the recycle delay based on previous experience in running ^{33}S NMR experiments on proton-containing systems in our laboratory. All ^{33}S experiments were run for 20000 scans, resulting in acquisition times of about 24 h per spectrum.

In addition to the ^{33}S OPUS experiments, the ^{14}N NMR powder pattern was also obtained from taurine. The spectrum was obtained at 11.7 T using a 6 mm Varian probe and Bruker Avance III spectrometer and was referenced to NH_4Cl at 0 ppm. The WURST-QCPMG pulse sequence[38] was used, with a methodology reported elsewhere.[39,40] The spectrum was acquired in 10 individual pieces separated by 200 kHz. For each piece, 128 echoes were acquired with 800 scans and a recycle delay of 1 s (total experimental time of 2 h). Echoes were coadded before processing.

3. RESULTS AND DISCUSSION

Optimal control theory is a mathematical method capable of finding the optimal solution in a system composed of a large number of variables, and has been previously used in numerous NMR applications[41−45] including the generation of excitation pulses.[35,46−48] In particular, it was recently shown that pulses generated in this way for a spin-3/2 nucleus can cause uniform signal enhancement via a complex and highly nonlinear PT mechanism, resulting in very accurate experimental CT lineshapes under static sample conditions.[35] Importantly, these pulses were shown to be surprisingly robust, performing well over a range of RF powers and offsets. While being numerically optimized for a very specific set of NMR parameters, such pulses still achieved uniform signal enhancement on samples whose NMR parameters differed significantly from those used for the optimization. This fact is crucial for the work described here because we have optimized pulses using a set of interaction parameters calculated from a (presumably) imperfect crystal structure, with the aim of subsequently assessing/refining it. If OPUS pulses only worked when the optimization parameters matched exactly with the experimental results, then no new information could be gained from using them.

An OPUS pulse optimized for the calculated ^{33}S NMR parameters (under 10 kHz MAS conditions at 11.7 T) is shown in Figure 2a. The pulse is 200 μs in length and consists of 800 individual elements, each of constant amplitude and phase (values listed in the Supporting Information). Due to the relatively long duration of this pulse, the amplitude ν_1 was restricted to a maximum value of 30 kHz, and the resultant mean amplitude of the pulse is 20.4 kHz. Both the amplitude and phase are clearly very strongly modulated and offer little hint as to the function of the pulse. As previously shown,[35] it is instructive to examine such a pulse using time-resolved Fourier analysis (Figure 2b). The frequencies of the modulations across the duration of the pulse are clustered within ±0.8 MHz of the RF transmitter frequency (set to the ^{33}S isotropic shift), with a noticeable gap present at the center where the CT is located. This clustering is perhaps not surprising when the shape of the calculated static ST powder pattern (shown on the right in Figure 2b) is considered. The high value of η_Q means that the STs are of highest intensity in the regions close to the CT, and irradiating these regions would be the most efficient way of exciting the entire ST manifold. Components of the ST pattern at the outermost edges (corresponding to particular crystallite orientations) will be passed through the central region by the rotation of the sample, resulting in a RAPT-like process.[25] As with previous excitation pulses generated using OCT,[35] modulation frequencies are absent from the CT region until the very end of the pulse, where the enhanced CT polarization is converted to observable single-quantum coherence. Another pulse, optimized for static conditions using the same ^{33}S parameters, was analyzed in the same way and showed a similar range of modulation frequencies (see Supporting Information).

The MAS and static ^{33}S NMR spectra obtained from taurine using the OPUS and control experiments are shown in Figure 3. The OPUS pulses resulted in significant signal enhancements relative to the control experiments (a factor of 2.26 for the MAS experiment and 1.78 for the static). This level of ^{33}S signal enhancement is slightly higher than that previously obtained using PT techniques after experimental optimization (ca. 1.9 on average) on samples with much smaller C_Q values.[22,23] It should be noted here that our comparison of the OPUS and control experiments is in fact biased in favor of the latter due to the fact that the control experiments exploited the knowledge of the calculated isotropic shift, which would otherwise not have been known. The greater enhancement factor in the MAS experiment can be attributed to several related factors. The element size for the MAS OPUS pulse is 0.25 μs compared with 0.1 μs for the static version, so the MAS pulse is likely reproduced more accurately by the spectrometer. This larger element size also restricts any amplitude and phase modulations of the MAS pulse to a narrower range of frequencies, meaning that inherent experimental bandwidth limitations (such as the probe quality factor) will be less detrimental to the performance of the pulse. Lastly, the MAS process itself causes a modulation of the ST frequencies as mentioned above, providing a further "degree of freedom" for the MAS OPUS pulse to achieve the PT.

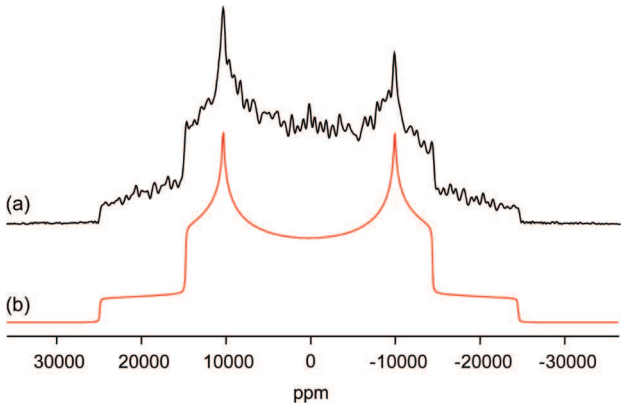

Figure 4. (a) ^{14}N NMR spectrum obtained from taurine using the (experimentally optimized) WURST-QCPMG pulse sequence.[38,39] (b) Fitted simulation (made in Dmfit),[49] which resulted in ^{14}N parameters of δ_{iso} = 200(100) ppm, C_Q = 1.19(1) MHz, and η_Q = 0.18(1). Uncertainties were estimated visually by the quality of fit, and CSA effects were neglected. The apparent slope in intensity, increasing toward higher frequencies, is a common phenomenon in ultrawideline NMR spectra, has been commented upon before,[11] and did not hinder the fit.

As well as providing a considerable gain in signal, the OPUS experiments resulted in powder patterns that could be simulated with good accuracy (Figure 3), thus, allowing an experimental determination of the ^{33}S NMR parameters (Table 1). The C_Q, η_Q, and δ_{iso} values were obtained from the MAS spectrum in which chemical shift anisotropy (CSA) effects are absent and were then fixed in the simulation of the static pattern from which the CSA parameters (Ω and κ) and Euler angles (α, β, γ) were determined. The agreement between the experimental parameters and those used to optimize the pulses is not bad (Table 1), and the discrepancies serve as a further demonstration of the flexibility of pulses optimized using OCT.

The information obtained from these experiments, in the form of the experimental ^{33}S NMR parameters, may then be used to evaluate the various other reported crystal structures of taurine by comparison with the parameters calculated from each structure using DFT. Calculated isotropic chemical shifts are prone to systematic errors since they are calculated relative to a bare nucleus, the experimental shift of which cannot be measured. Euler angles can also be prone to large uncertainties as well as the existence of multiple, equivalent sets of values. We therefore consider the ^{33}S EFG and shielding tensor parameters

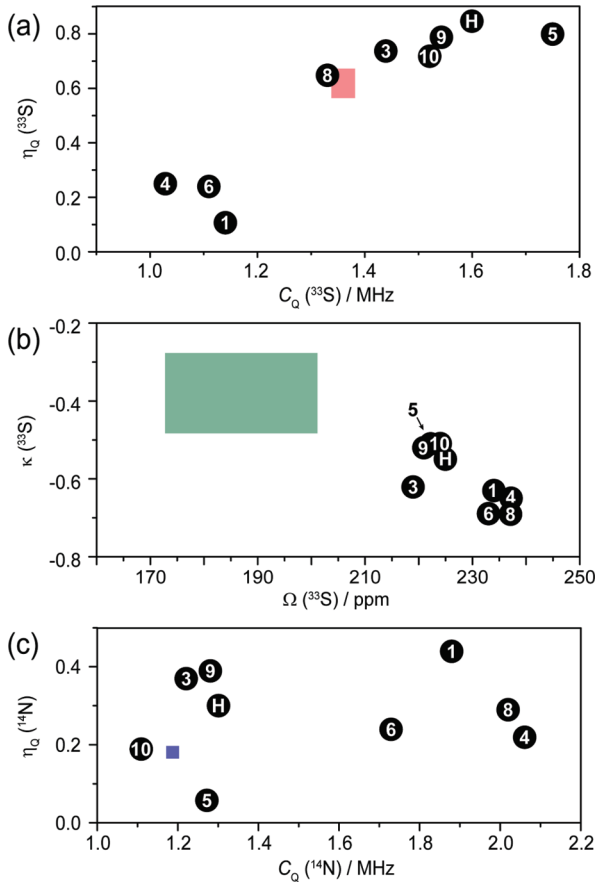

Figure 5. Calculated parameters for (a) the ^{33}S quadrupolar interaction, (b) the ^{33}S CSA, and (c) the ^{14}N quadrupolar interaction in taurine. Numbers *n* correspond to the CCSD code of the structure used (TAURIN*n*). H corresponds to the values used in the generation of the OPUS pulses, obtained after proton optimization of structure 3. Colored boxes represent the ranges of experimental values bound by the experimental uncertainties.

C_Q, η_Q, Ω, and κ in the evaluation. In addition to the ^{33}S data, experimentally determined ^{14}N EFG parameters measured from the static ^{14}N powder pattern (Figure 4) are also considered.

The comparison between the experimental NMR parameters and those calculated from the various taurine structures[31,50−56] are shown as graphical plots in Figure 5 (all calculated parameters are given in the Supporting Information). Three of the structures, TAURIN03, 09, and 10, give a better agreement with the experimental parameters than the others. These correspond to a room-temperature (partially deuterated) neutron diffraction structure[50] and two very recent XRD structures determined at 120 K and room temperature, respectively.[51] An optimization of the proton positions was conducted on all three of these structures, which resulted in extremely similar calculated parameters to those given in Table 1 ("H" in Figure 5, see Supporting Information for exact values), giving a poorer overall match to the experimental values than the unoptimized structures. In addition, a full optimization of structure 1 was conducted with all atomic positions allowed to vary. This also resulted in a poorer match with experiment (see Supporting Information for exact numbers). Interestingly, it can be seen in Figure 5 that the neutron structure (TAURIN03) gives the best match for the experimental parameters describing the magnitudes of the quadrupolar

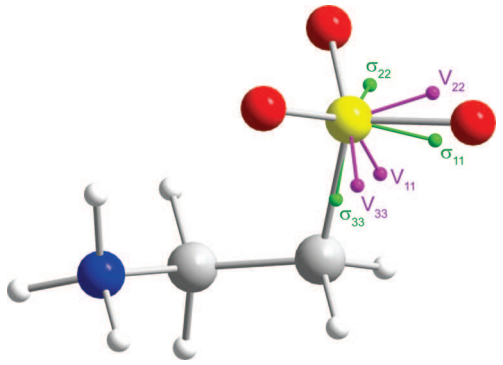

Figure 6. ^{33}S EFG and CSA tensor orientations calculated from the neutron diffraction structure (TAURIN03).

and CSA interactions (C_Q and Ω), while TAURIN10 gives the best match for the asymmetries of these interactions (η_Q and κ). The neutron structure also gives the best match for the Euler angle β, which is the angle between the largest principal components of the EFG and CSA tensors (see Supporting Information). In general, the interaction magnitudes will have smaller associated uncertainties (in both experimental measurements and calculations) than the asymmetry parameters, thus, on the basis of these results we conclude that the neutron diffraction structure[50] is the most accurate of those reported. This is perhaps not surprising given that neutron diffraction structures are well-known to provide more accurate proton positions than XRD experiments.

Finally, the molecular-frame orientations of the ^{33}S EFG and CSA tensors calculated from the unoptimized neutron diffraction structure are shown in Figure 6. The most shielded component of the CSA tensor, σ_{33}, is aligned within 3° of the S−C bond, with σ_{11} pointing in the approximate direction of the S−O2 bond. The largest component of the EFG tensor, V_{33}, is aligned very close to the S−O1 bond (<5°), with V_{22} pointing in the approximate direction of the S−O2 bond.

4. SUMMARY

We have presented a strategy for the a priori optimization of SSNMR experiments for insensitive half-integer quadrupolar nuclei. NMR parameters are predicted from a crystal structure by density functional theory and used to generate excitation pulses with optimal control theory. This approach was used to acquire natural abundance ^{33}S NMR spectra from taurine without the need for any experimental optimization whatsoever, and a significant signal enhancement was achieved under both static and MAS conditions. Such a strategy can be implemented with freely available software and could provide a route to the natural abundance study of other low-sensitivity quadrupolar nuclei such as ^{17}O, ^{25} Mg, or ^{43}Ca on which established PT methods may be difficult to optimize experimentally without the use of isotopically enriched samples. The ^{33}S (and ^{14}N) experimental parameters were subsequently used in the assessment of the various crystal structures of taurine, which also serves to highlight the role that quadrupolar nuclei can play in NMR crystallography.

■ ASSOCIATED CONTENT

Supporting Information. Reported taurine crystal structures, definitions of NMR parameters, analysis of the static OPUS

dx.doi.org/10.1021/jp111531e |*J. Phys. Chem. A* 2011, 115, 747–752

pulse, all DFT calculation results, and lists of the OPUS pulse amplitudes and phases. This material is available free of charge via the Internet at http://pubs.acs.org.

AUTHOR INFORMATION

Corresponding Author

*To whom correspondence should be addressed. E-mail: luke.odell@nrc-cnrc.gc.ca.

ACKNOWLEDGMENT

Access to the CASTEP software was provided by the National Ultra-High Field NMR Facility for Solids, Ottawa (www.nmr900.ca).

REFERENCES

(1) *NMR Crystallography*; Harris, R. K., Wasylishen, R. E., Duer, M. J., Eds.; John Wiley and Sons, Ltd.: New York, 2009.
(2) Salager, E.; Day, G. M.; Stein, R. S.; Pickard, C. J.; Elena, B.; Emsley, L. *J. Am. Chem. Soc.* **2010,** *132*, 2564.
(3) Harris, R. K.; Hodgkinson, P.; Zorin, V.; Dumez, J.-N.; Elena-Herrmann, B.; Emsley, L.; Salager, E.; Stein, R. S. *Magn. Reson. Chem.* **2010** DOI: 10.1002/mrc.2636.
(4) Brouwer, D. H. *J. Am. Chem. Soc.* **2008,** *130*, 6306.
(5) Zhou, B.; Giavani, T.; Bildsøe, H.; Skibsted, J.; Jakobsen, H. J. *Chem. Phys. Lett.* **2005,** *402*, 133.
(6) Widdifield, C. M.; Bryce, D. L. *Phys. Chem. Chem. Phys.* **2009,** *11*, 7120.
(7) Pickard, C. J.; Mauri, F. *Phys. Rev. B* **2001,** *63*, 245101.
(8) Profeta, M.; Mauri, F.; Pickard, C. J. *J. Am. Chem. Soc.* **2003,** *125*, 541.
(9) Clark, S. J.; Segall, M. D.; Pickard, C. J.; Hasnip, P. J.; Probert, M. J.; Refson, K.; Payne, M. C. *Z. Kristallogr.* **2005,** *220*, 567.
(10) Yates, J. R.; Pickard, C. J.; Mauri, F. *Phys. Rev. B* **2007,** *76*, 024401.
(11) Brouwer, D. H.; Darton, R. J.; Morris, R. E.; Levitt, M. H. *J. Am. Chem. Soc.* **2005,** *127*, 10365.
(12) Pickard, C. J.; Salager, E.; Pintacuda, G.; Elena, B.; Emsley, L. *J. Am. Chem. Soc.* **2007,** *129*, 8932.
(13) Salager, E.; Stein, R. S.; Pickard, C. J.; Elena, B.; Emsley, L. *Phys. Chem. Chem. Phys.* **2009,** *11*, 2610.
(14) Woodley, S. M.; Catlow, R. *Nat. Mater.* **2008,** *7*, 937.
(15) MacKenzie, K. J. D.; Smith, M. E. *Multinuclear Solid-State NMR of Inorganic Materials*; Pergamon: Elmsford, NY, 2002.
(16) Duer, M. J. *Solid-State NMR Spectroscopy*; Blackwell: Cambridge, MA, 2004.
(17) Wagler, T. A.; Daunch, W. A.; Rinaldi, P. L.; Palmer, A. R. *J. Magn. Reson.* **2003,** *161*, 191.
(18) Wagler, T. A.; Daunch, W. A.; Panzner, M.; Youngs, W. J.; Rinaldi, P. L. *J. Magn. Reson.* **2004,** *170*, 336.
(19) Couch, S.; Howes, A. P.; Kohn, S. C.; Smith, M. E. *Solid State Nucl. Magn. Reson.* **2004,** *26*, 203.
(20) Haase, J.; Conradi, M. S. *Chem. Phys. Lett.* **1993,** *209*, 287.
(21) Siegel, R.; Nakashima, T. T.; Wasylishen, R. E. *Concepts Magn. Reson., Part A* **2005,** *26*, 47.
(22) Hansen, M. R.; Brorson, M.; Bildsøe, H.; Skibsted, J.; Jakobsen, H. J. *J. Magn. Reson.* **2008,** *190*, 316.
(23) O'Dell, L. A.; Klimm, K.; Freitas, J. C. C.; Kohn, S. C.; Smith, M. E. *Appl. Magn. Reson.* **2008,** *35*, 247.
(24) Kentgens, A. P. M.; Verhagen, R. *Chem. Phys. Lett.* **1999,** *300*, 435.
(25) Yao, Z.; Kwak, H.-T.; Sakellariou, D.; Emsley, L.; Grandinetti, P. J. *Chem. Phys. Lett.* **2000,** *327*, 85.
(26) Siegel, R.; Nakashima, T. T.; Wasylishen, R. E. *Chem. Phys. Lett.* **2004,** *388*, 441.
(27) Larsen, F. H.; Jakobsen, H. J.; Ellis, P. D.; Nielsen, N. C. *J. Phys. Chem. A* **1997,** *101*, 8597.
(28) Siegel, R.; Nakashima, T. T.; Wasylishen, R. E. *Concepts Magn. Reson., Part A* **2005,** *26*, 62.
(29) Schurko, R. W.; Hung, I.; Widdifield, C. M. *Chem. Phys. Lett.* **2003,** *379*, 1.
(30) Pfrommer, B. G.; Cote, M.; Louie, S. G.; Cohen, M. L. *J. Comput. Phys.* **1997,** *131*, 233.
(31) Okaya, Y. *Acta Crystallogr.* **1966,** *21*, 726.
(32) Adiga, S.; Aebi, D.; Bryce, D. L. *Can. J. Chem.* **2007,** *85*, 496.
(33) Bak, M.; Rasmussen, J. T.; Nielsen, N. C. *J. Magn. Reson.* **2000,** *147*, 296.
(34) Tošner, Z.; Vosegaard, T.; Kehlet, C.; Khaneja, N.; Glaser, S. J.; Nielsen, N. C. *J. Magn. Reson.* **2009,** *197*, 120.
(35) O'Dell, L. A.; Harris, K. J.; Schurko, R. W. *J. Magn. Reson.* **2010,** *203*, 156.
(36) Vosegaard, T.; Skibsted, J.; Bildsøe, H.; Jakobsen, H. J. *J. Phys. Chem.* **1995,** *99*, 10731.
(37) Moudrakovski, I.; Lang, S.; Patchkovskii, S.; Ripmeester, J. *J. Phys. Chem. A* **2010,** *114*, 309.
(38) O'Dell, L. A.; Schurko, R. W. *Chem. Phys. Lett.* **2008,** *464*, 97.
(39) O'Dell, L. A.; Schurko, R. W. *J. Am. Chem. Soc.* **2009,** *131*, 6658.
(40) O'Dell, L. A.; Schurko, R. W. *Phys. Chem. Chem. Phys.* **2009,** *11*, 7069.
(41) Glaser, S. J.; Schulte-Herbrüggen, T.; Sieveking, M.; Schedletzky, O.; Nielsen, N. C.; Sørensen, O. W.; Griesinger, C. *Science* **1998,** *280*, 421.
(42) Khaneja, N.; Li, J.-S.; Kehlet, C.; Luy, B.; Glaser, S. J. *Proc. Natl. Acad. Sci. U.S.A.* **2004,** *101*, 14742.
(43) Khaneja, N.; Reiss, T.; Kehlet, C.; Schulte-Herbrüggen, T.; Glaser, S. J. *J. Magn. Reson.* **2005,** *172*, 296.
(44) Kehlet, C.; Sivertsen, A. C.; Bjerring, M.; Reiss, T. O.; Khaneja, N.; Glaser, S. J.; Nielsen, N. C. *J. Am. Chem. Soc.* **2004,** *126*, 10202.
(45) Vosegaard, T.; Kehlet, C.; Khaneja, N.; Glaser, S. J.; Nielsen, N. C. *J. Am. Chem. Soc.* **2005,** *127*, 13768.
(46) Skinner, T. E.; Reiss, T.; Luy, B.; Khaneja, N.; Glaser, S. J. *J. Magn. Reson.* **2003,** *163*, 8.
(47) Skinner, T. E.; Reiss, T. O.; Luy, B.; Khaneja, N.; Glaser, S. J. *J. Magn. Reson.* **2004,** *167*, 68.
(48) Kobzar, K.; Skinner, T. E.; Khaneja, N.; Glaser, S. J.; Luy, B. *J. Magn. Reson.* **2004,** *170*, 236.
(49) Massiot, D.; Fayon, F.; Capron, M.; King, I.; Le Calvé, S.; Alonso, B.; Durand, J. O.; Bujoli, B.; Gan, Z.; Hoatson, G. *Magn. Reson. Chem.* **2002,** *40*, 70.
(50) Briant, C. E.; Jones, D. W. *J. Chem. Crystallogr.* **1997,** *27*, 481.
(51) Beukes, J. A.; Mo, F.; van Beek, W. *Phys. Chem. Chem. Phys.* **2007,** *9*, 4709.
(52) Sutherland, H. H.; Young, D. W. *Acta Crystallogr.* **1963,** *16*, 897.
(53) Görbitz, C. H.; Prydz, K.; Ugland, S. Taurine *Acta Crystallogr., Sect. C* **2000,** *56*, 23.
(54) Hibbs, D. E.; Austin-Woods, C. J.; Platts, J. A.; Overgaard, J.; Turner, P. *Chem.—Eur. J.* **2003,** *9*, 1075.
(55) Hasegawa, T.; Kumai, R.; Takahashi, Y.; Tokura, Y.; Sawa, H. *Rev. Sci. Instrum.* **2005,** *76*, 073903.
(56) Tasdemir, D.; Topaloglu, B.; Perozzo, R.; Brun, R.; O'Neill, R.; Carballeira, N. M.; Zhang, X.; Tonge, P. J.; Linden, A.; Rüedi, P. *Bioorg. Med. Chem.* **2007,** *15*, 6834.